Assiut University Journal of Multidisciplinary Scientific Research (AUNJMSR)
Faculty of Science, Assiut University, Assiut, Egypt.
Printed ISSN 2812-5029
Online ISSN 2812-5037
Vol. 54(2): 209- 228 (2025)
https://aunj.journals.ekb.eg

Numerical Study of Sutterby Nanofluid Flow Over Unstretched Horizontal Cylinder Enveloped by Heated Tissue

R.S. Kamel[1,2,*], A.M. Ismaeel[1,3], F.M. Hady[1]
[1]Department of Mathematics, Faculty of Science, Assiut University, Assiut, Egypt
[2]Higher Institute of Engineering and Technology, New Minya, Egypt
[3]Faculty of Basic Sciences, King Salman International University, South Sinai, Egypt

[*]Corresponding Author: rehabshaher78@gmail.com

ARTICLE INFO

Article History:
Received: 2024-12-19
Accepted: 2025-01-20
Online: 2025-04-27

Keywords:
Sutterby nanofluid, interstitial fluid velocity, hyperthermia therapy, Brownian motion, thermophoresis.

ABSTRACT

This study presents a mathematical model for the heat transfer behavior of Sutterby nanofluid on the surface of an unexpanded horizontal cylinder exposed to an external heat source and a magnetic field. A nonlinear differential system was formulated and solved numerically using MATLAB's bvp4c solver. The model investigates the effects of Brownian motion, thermophoresis, interstitial fluid velocity, and tissue thermal absorption on nanoparticle (NPs) distribution and fluid temperature.

The most important result of this study is that increasing cylinder curvature (K) enhances NPs accumulation and raises interstitial fluid temperature, improving the potential for thermal therapy. However, higher radiation parameter R_d reduces NPs concentration, which could negatively affect treatment efficacy. These results emphasize the importance of optimizing physical parameters—such as curvature, radiation, and fluid velocity—in enhancing the effectiveness of nanofluid-based thermal therapy. The study provides valuable insights for clinical applications, highlighting the need to balance these factors to maximize treatment outcomes.

1. INTRODUCTION

Nanofluid is a mixture of solid metal particles dispersed in base fluids. Common base fluids include water, ethylene glycol and oil are usually used to prepare nanofluids. Nanoparticles (NPs) can exist in various forms, including metals, nitrides, carbon nanotubes, and metallic oxides, each possess unique properties and applications. Nanofluids show better thermal conductivity than standard base fluids, which has generated substantial interest from researchers and scientists in the last decade. Their distinctive characteristics enable a wide range of applications in areas such as energy, healthcare, and electronics, and ongoing research continues to broaden their potential across diverse industries. The concept of nanofluids was initially introduced by Choi [1], while Buongiorno [2] conducted a thorough examination of convective heat transport in these fluids.

In recent years, non-Newtonian fluids have gained growing interest because of their extensive applications in industry and engineering. These fluids find applications in several processes, including the production of plastic films, the annealing and thinning of wires, and the condensation of liquid films. However, the equations of Navier-Stokes do not fully account for all characteristics of non-Newtonian fluids, prompting the development of various fluid models. One example is the Sutterby Fluid Model introduced by Sutterby et al. [3]. Guha et al. [4] investigated the convective flow of Sutterby fluids over a horizontal thermally stable plate, whereas Bijjan et al. [5] focused on the thermal transport properties in power law fluid flow involving a stretched cylinder. Meanwhile, Abdelsalam et al. [6] analysed the dynamics of non-Newtonian Sutterby nanofluid flow produced by stretched cylinders with suspended microorganisms. Rahman et al. [7] investigated the irreversibility of Sutterby nanofluid flow using a stretched cylinder. The effects of important factors on velocity, entropy, temperature, Bejan number, and concentration were investigated. The findings revealed that the velocity field diminishes with an increase in porosity and Forchheimer factors. Moreover, the graphs for velocity and temperature revealed an inverse relationship with the magnetic parameters. The higher Schmidt number led to a decline in the concentration distribution, while the entropy generation amplified by the magnetic parameter and Brinkman number. Aldabesh et al. [8] studied the thermal characteristics of Sutterby nanofluids, taking into account microorganisms affected by the stretched cylinder. Their analysis included nonlinear thermal radiation, Darcy resistance, and activation energy to evaluate thermal potential. Results were presented for both the stretched cylinder and stationary plate. The findings revealed that the Darcy resistance parameter significantly increased velocity for stretched cylinders, while the Sutterby fluid parameter and buoyancy ratio parameter contributed to a decrease in velocity. Moreover, a higher sponginess parameter enhanced the temperature profile, making it more effective for extending the cylinder. Meanwhile, Fazal et al. [9] focused on mixed convection magnetohydrodynamic flow of Casson nanomaterials through a stretchy cylinder, calculating and examining critical engineering quantities such as surface drag force, heat transfer rate, density number, and Sherwood number. The results show that fluid velocity decreases in the case of increasing curvature, Casson fluid substance, Hartmann number, and permeability parameter. Zakir et al. [10] presented a comparative analysis of the convective movement of Williamson liquid over cylinders and sheets. They simulated heat transfer within both geometries, considering factors such as convection, viscous dissipation, Joule heating, and heat sources. The findings revealed that liquid flow and concentration were more significant in cylinders than in sheets. Additionally, it was observed that the Prandtl, Biot, and curvature variables increased the heat transfer rate, whereas the Eckert and heat source variables had the opposite effect. Bilal et al. [11] investigated the heat and mass transfer properties of Sutterby fluid affected by a magnetic field. They formulated the flow field equations in cylindrical coordinates using Darcy's resistance law. Their study incorporates graphical representations that highlight the effects of various physical parameters on the profiles of velocity, temperature, and concentration. Hayat et al. [12] investigated the influence of compliant walls on the peristaltic flow of Sutterby nanofluid in a vertical channel, incorporating a uniform magnetic field applied transversely. They also examined heat transfer effects under convective boundary conditions. Their findings indicated that the velocity and temperature distributions in Sutterby fluid exceeded those in viscous fluids, and that the radiation parameter contributed to a decrease in fluid temperature within the channel. Ehsan et al. [13] carried out analytical simulations of thermos-migration flow of nanofluid, focusing on the effects of thermal radiation and porous media. They found that the moving wedge significantly altered the flow pattern, with a notable decrease in velocity linked to a larger change in the magnetic constant. Ismaeel et al. [14] established a mathematical model to illustrate the microscale transport of heat and NPs in tissue adjacent to a vertical vessel. Their results indicated that the vessel pore size significantly impacts the tissue ability to transport heat. They identified that the heat flux at the outer boundary of the tissue and the fluid extravasation velocity are critical factors affecting the vessel heat dissipation. In a follow-up study, Ismaeel et al. [15] introduced a theoretical model to analyze NP movement and heat transfer in the tumor interstitium surrounding an inclined cylindrical blood vessel exposed to the magnetic field. They took into account the non-Newtonian properties of interstitial nanofluid in tumors to capture the nonlinear behavior of the fluid flow accurately. Their findings suggested that optimizing the delivery of NPs and managing tumor temperature could enhance tumor ablation through hyperthermia. Additionally, Kamel et al. [16] developed a theoretical model to investigate heat and mass transport in biological tissues subjected to a magnetic field, simulating thermal therapy for cancer treatment. Their predictions indicated that enhanced heat absorption by NPs raises tumor temperature, thereby improving treatment efficacy while reducing particle concentration. Ismaeel et al. [17] examined the use of a Newtonian nanofluid with suspended NPs to enhance heat and mass transfer in biological tissues under a magnetic field. The results indicate that increasing the heat source parameter significantly raises the interstitial temperature within tumors. This temperature increase, along with improved accumulation of NPs in the tumor, is essential for effective hyperthermia treatment. The findings provide important insights into optimizing thermal therapy for cancer treatment using nanofluids, potentially leading to better therapeutic outcomes.

In this manuscript, we explore the dynamics of Sutterby nanofluid flow around a horizontal cylinder in the presence of a magnetic field, focusing on how NPs migrate from nearby blood vessels to tissue exposed to elevated temperatures. We develop an innovative modelling approach for two-dimensional Sutterby fluid flow using boundary layer approximation. This allows for the transformation of complex partial differential equations (PDEs) into ordinary differential equations (ODEs), which solved numerically using MATLAB bvp4c solver, adhering to the necessary boundary conditions.

The manuscript is organized as follows: Section 1 (Introduction) provides an overview of magnetohydrodynamic nanofluids, their intrinsic thermal properties, and their applications in biomedicine. Section 2 details the physical model and its corresponding mathematical formulation. Section 3 outlines the approach used for the numerical solution. In Section 4, the results of the mathematical model are presented, along with a discussion of the findings. Finally, Section 5 concludes the paper.

2. MATERIALS AND METHODS

2.1 Mathematical Model

We analyse the two-dimensional Sutterby nanofluids flow via cylinder. The flow happens within an unstretched cylinder with radius R. Fig. 1 shows the physical configuration of the flow phenomena. The nanofluid transports past an unstretched and stationary cylinder. It is assumed that both the blood temperature (T_b) and NPs concentration (C_b) within the blood vessel remain constant. Furthermore, we demonstrate the migration of NPs from a nearby blood vessel to tissue subjected to high levels of heat. In this model, the extrinsic heat source, such as the magnetic field, is the main source of heat, transferring energy to the tissue surrounding the cylinder.

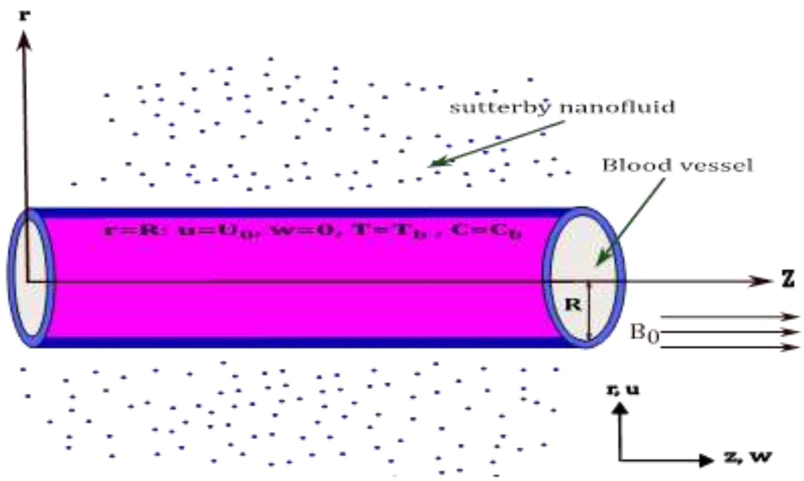

Figure 1: The physical domain.

The following partial differential equations (PDEs) represent flow, heat and mass transfer based on theorized assumptions [18].

$$\frac{\partial u}{\partial r}+\frac{u}{r}+\frac{\partial \mathrm{w}}{\partial \mathrm{z}}=0, \tag{1}$$

$$\left(u\,\frac{\partial w}{\partial r}+w\,\frac{\partial w}{\partial z}\right)=\frac{\nu}{2r}\,\frac{\partial w}{\partial r}+\frac{\nu}{2}\,\frac{\partial^2 w}{\partial r^2}-\frac{\nu m B^2}{4}\left(\frac{\partial w}{\partial r}\right)^2\frac{\partial^2 w}{\partial r^2}-\frac{\sigma B_0^2}{\rho}w+g\left[\beta_T\,(T-T_\infty)+\beta_c\,(C-C_\infty)\right], \tag{2}$$

$$\left(w\,\frac{\partial T}{\partial z}+u\,\frac{\partial T}{\partial r}\right)=\frac{k}{\rho\,c_p}\,\left(\frac{\partial^2 T}{\partial r^2}+\frac{1}{r}\,\frac{\partial T}{\partial r}\right)+\tau\left[D_B\frac{\partial T}{\partial r}\frac{\partial C}{\partial r}+\frac{D_T}{T_\infty}\left(\frac{\partial T}{\partial r}\right)^2\right]+\frac{\sigma B_0^2}{\rho}w^2+\frac{16\,\sigma^* T_\infty^3}{3\rho\,c_p k^*}\,\frac{\partial^2 T}{\partial r^2}+\frac{SAR}{\rho c_p}(C-C_\infty), \tag{3}$$

$$\left(w\,\frac{\partial C}{\partial z}+u\,\frac{\partial C}{\partial r}\right)=D_B\,\frac{1}{r}\frac{\partial}{\partial r}\left[r\,\frac{\partial C}{\partial r}\right]+\frac{D_T}{T_\infty}\frac{1}{r}\frac{\partial}{\partial r}\left[r\,\frac{\partial T}{\partial r}\right]. \tag{4}$$

In this context, (u, w) signify the components of fluid velocity in the radial and axial directions, respectively, and C denotes the concentration of NPs. In addition, ν represents kinematics viscosity, D_B represents Brownian motion, D_T represents thermophoresis coefficient, m is the power law index, B is the characteristic Time, ρ_f represents fluid density, SAR reflects the rate at which biological tissue absorbs energy, and τ represents the ratio of the heat capacity between the NPs and the base fluid, which defined as $\tau=\frac{(\rho c_p)_p}{(\rho c_p)_f}$.

The following are the boundary conditions governing the model:

$$\text{At } r = R: \quad u = U_0, \quad w = 0, \; T = T_b, \quad C = C_b \tag{5}$$

$$\text{as } r \to \infty: \quad \frac{1}{r}\frac{\partial}{\partial r}(ru) \to 0, \quad uT - \left(\frac{k}{\rho c_p} + \frac{16\,\sigma^* T_\infty^3}{3(\rho c_p)k^*}\right)\frac{\partial T}{\partial r} \to Q_H,$$
$$uC - D_B\frac{\partial C}{\partial r} - \frac{D_T}{T_\infty}\frac{\partial T}{\partial r} \to \bar{K}, \tag{6}$$

where R is the cylinder's radius.

We use the following analogous transformations [18] to convert the system of PDEs (1-6) into a system of ordinary differential equations (ODEs):

$$\eta = \sqrt{\frac{U_0}{\upsilon L}}\left(\frac{r^2 - R^2}{2R}\right). \tag{7}$$

$$u = \frac{-R}{r}\sqrt{\frac{\upsilon U_0}{L}}\; f(\eta) \quad , \qquad w = \frac{z\,U_0}{L}\; f'(\eta). \tag{8}$$

Moreover, the following definitions apply to dimensionless temperature and NP concentration:

$$\theta(\eta) = \frac{T - T_\infty}{T_b - T_\infty} \quad , \qquad \varphi(\eta) = \frac{C - C_\infty}{C_b - C_\infty}. \tag{9}$$

By applying the transformations (7-9) to the system of equations (Eqs. 1-6) we obtain:

$$(1 + 2K\eta)f''' + 2Kf'' + 2ff'' - 2f'^2 - 2\beta_1\, R_e K\,(1 + 2K\eta)\, f''^3 -$$
$$2\beta_1\, R_e(1 + 2K\eta)^2\, f''^2 f''' - 2\lambda(\theta + N\varphi)f^2 f'' - 2Mf' = 0, \tag{10}$$

$$(1 + 2K\eta)\theta'' + 2K\theta' + P_r\, f\theta' + (1 + 2K\eta)\, N_b\, P_r\, \theta'\, \varphi' +$$
$$(1 + 2K\eta)\, N_t\;\, P_r\, \theta'^2 + P_r\, M\, E_c\, f'^2 + \frac{4}{3}R_d\,[(1 + 2K\eta)\theta'' + K\theta'] + \tag{11}$$
$$\lambda^* \frac{Nb}{Nt}\, P_r\, \varphi(\eta) = 0,$$

$$(1 + 2K\eta)\varphi'' + 2K\varphi' + \frac{Nt}{Nb}[(1 + 2K\eta)\theta'' + 2K\theta'] + S_c\, P_r\, f\varphi' = 0. \tag{12}$$

where $K = \frac{1}{R}\sqrt{\frac{\upsilon\, L}{U_0}}$ is the curvature parameter of the cylinder, $M = \frac{\sigma\, L\, B_0^2}{\rho U_0}$ is the magnetic field parameter, $\lambda = \frac{G_{r_z}}{(Re_z)^2}$, $\beta_1 = \frac{m\, B^2\, U_0^2}{4L^2}$, $G_{r_z} = \frac{g\, \beta_T\,(T - T_\infty)\, z^3}{\nu^2}$ is the thermal Grashof number , $Re_z = \frac{W_w\, z}{\nu}$ is the Reynolds number, $R_d = \frac{4\,\sigma^* T_\infty^3}{k\, k^*}$ is the thermal radiation parameter , $S_c = \frac{\upsilon}{D_B}$ is the Schmidt number, $N = \frac{\beta_c (C_b - C_\infty)}{\beta_T (T_b - T_\infty)}$, $E_c = \frac{U^2{}_w}{(c_p)_f\, (T_b - T_\infty)}$ is the Eckert number $P_r = \frac{\upsilon \rho c_p}{k}$ is the Prandtl number, $N_b = \frac{\tau D_B (C_b - C_\infty)}{\upsilon}$ is the Brownian motion parameter, $N_t = \frac{\tau D_T\, (T_b - T_\infty)}{\upsilon\, T_\infty}$ is the thermophoresis parameter and finally, $\lambda^* = \frac{D_T\, SAR\, L}{U_0\, D_B\, T_\infty\, (\rho c_p)}$ is the specific heat parameter, $\overline{K}$ is the certain constant related to mass transfer, U_0 is the radial Velocity at the Boundary, W_w is the velocity in the axial direction.

By applying the dimensionless transformations (7–9), the boundary conditions (Eqs. (5 & 6)) can be expressed as follows:

$$At\, \eta = 0: \quad f(0) = -\gamma, \quad f'(\eta) = 0, \quad \theta(\eta) = 1, \quad \varphi(\eta) = 1, \tag{13}$$

$$as\, \eta \to \infty: \quad f'(\infty) = 0, \quad f\,(\theta + \xi_1)\, \frac{\sqrt{S_c}}{(1+2K\eta)^{0.5}} + \frac{\sqrt{S_c}}{P_r}\left(1 + \frac{4}{3}\, R_d\right)(1 + 2K\eta)^{0.5}\, \theta' \to -Q_H^*, \tag{14}$$

$$f(\varphi + \xi_2)\, \frac{\sqrt{S_c}}{(1 + 2K\eta)^{0.5}} + \frac{(1 + 2K\eta)^{0.5}}{\sqrt{S_c}}\left(\varphi' + \frac{Nt}{Nb}\theta'\right) \to -K_H^*. \tag{15}$$

We may estimate the dimensionless heat flow via the blood vessel walls using equation (14)

$$Q_H^*|_{\eta=0} = \gamma\, (1 + \xi_1)\, \sqrt{S_c} - \frac{\sqrt{S_c}}{P_r}\left(1 + \frac{4}{3}\, R_d\right)\, \theta' \tag{16}$$

Where $K_H^* = \frac{L^{0.5}\, \overline{K}}{U_0^{0.5}\, D_B^{0.5}\, (C_b - C_\infty)}$, $Q_H^* = \frac{L^{0.5}\, Q_H}{U_0^{0.5}\, D_B^{0.5}\, (T_b - T_\infty)}$ $\xi_1 = \frac{T_\infty}{T_b - T_\infty}$, $\xi_2 = \frac{C_\infty}{C_b - C_\infty}$.

The physical quantities, including the skin friction coefficient C_f and the local Nusselt number N_u, are defined in their dimensionless form as follows:

$$C_f = -\frac{(\tau_w)_{r=R}}{\rho_f W_w^2}, \qquad N_u = \frac{z\, q_w}{k\, (T_b - T_\infty)}, \tag{17}$$

where

$$\tau_w = (\mu)\left[\frac{dw}{dr}\right]^2_{r=R}, q_w = -k\left(1 + \frac{16\,\sigma^* T_\infty^3}{3kk^*}\right)\left[\frac{dT}{dr}\right]_{r=R}. \tag{18}$$

q_w represents the surface heat flux of the unstretched cylinder, while τ_w indicates the shear stress. When Eq. (18) is substituted into Eq. (17), the local Nusselt number and skin friction are expressed as follows:

$$C_f\, Re_z^{1/2} = -f''(0), \quad N_u Re_z^{-1/2} = -\left(1 + \frac{4}{3}R_d\right)\theta'(0). \tag{19}$$

2.2 Method of solution

We employed the built-in MATLAB function *bvp4c*, which is specifically designed to solve boundary value problems, to tackle the system of nonlinear and coupled ODEs (10–12) subject to the boundary conditions (13-15).

For this purpose, we introduced the following new variables:

$$s_1 = f, s_2 = f', s_3 = f'', s_4 = \theta, s_5 = \theta', s_6 = \varphi, s_7 = \varphi' \tag{20}$$

Thus, the equations (10–12) and (13–15) can be expressed as follows:

$$s_1' = s_2, s_2' = s_3,$$

$$s_3' = \frac{1}{(1+2K\eta) - 2\beta_1 R_e (1+2K\eta)^2 s_3^2}\left[-2\,K\,s_3 - 2s_1\,s_3 + 2s_2^2 + 2\,\beta_1\,R_e K(1 + 2K\eta)s_3^3 + 2M\,s_2 - 2\lambda\,(s_4 + N\,s_6)\right],$$

$$s_5' = \frac{-P_r}{(1+2K\eta)(1+\frac{4}{3}R_d)}\, s_1 s_5 - \frac{-2K}{(1+2K\eta)\left(1+\frac{4}{3}R_d\right)}\, s_5 - \frac{-P_r\,N_b}{\left(1+\frac{4}{3}R_d\right)} s_5\, s_7 - \frac{-P_r\,N_t}{\left(1+\frac{4}{3}R_d\right)}\, s_5^2 - \frac{P_r\,M\,E_c}{(1+2K\eta)\left(1+\frac{4}{3}R_d\right)}\, s_2^2 - \frac{\lambda^*\,P_r\,N_b}{(1+2K\eta)\left(1+\frac{4}{3}R_d\right)N_t}\, s_6 - \frac{\frac{4}{3}R_d\,K}{(1+2K\eta)\left(1+\frac{4}{3}R_d\right)}\, s_5, \tag{21}$$

$$s_7' = \frac{-2K}{(1+2K\eta)} s_7 - \frac{N_t}{N_b}\left[\, s_5' + \frac{2K}{(1+2K\eta)}\, s_5\right] - \frac{S_c}{(1+2K\eta)} s_1\, s_7\,.$$

The boundary conditions (13-15) can be expressed as follows:

$$At\ \eta = 0: \quad s_1 = -\gamma, \quad s_2 = 0, \quad s_4 = 1, \ s_6 = 1.$$

$$At\ \eta = \infty: \quad s_2 = 0, \quad s_1(s_4 + \xi_1)\frac{\sqrt{S_c}}{(1+2K\eta)^{0.5}} + \frac{\sqrt{S_c}}{P_r}\left(1 + \frac{4}{3}R_d\right)(1 + 2K\eta)^{0.5}\, s_5 = -Q_H^*\ , \tag{22}$$

$$s_1(s_6 + \xi_2)\frac{\sqrt{S_c}}{(1+2K\eta)^{0.5}} + \frac{(1+2K\eta)^{0.5}}{\sqrt{S_c}}\left(s_7 + \frac{N_t}{N_b}s_5\right) = -K_H^* \ .$$

The initial values of the model variables are as follows:

$$s_1 = s_2 = s_3 = s_4 = s_5 = s_6 = s_7 = 0.$$

We use the built-in MATLAB function *bvp4c* to solve the system of first-order ODEs [19]. Table 1 lists the parameter values that were selected for this investigation. In the following section, we will examine the results of the mathematical model.

Table 1: The basic Parameters Values

Parameter	value	Parameter	Value	Parameter	value
$\boldsymbol{\beta_1}$	0.5	N_t	0. 1	ξ_2	0.01
$\boldsymbol{\gamma}$	0.1	N_b	0.1	λ	0.1
$\mathbf{Q_H^*}$	0. 03	P_r	1.5	K	5
$\mathbf{K_H^*}$	0.03	R_e	0.01	M	0.3
$\mathbf{E_c}$	0.2	S_c	1.5		
$\boldsymbol{\lambda^*}$	0.05	ξ_1	0.01		
N	0.1	R_d	0		

Table 2: Comparative evaluation of values with the extant literature of $\theta''(0)$, under conditions $\beta = E_c = 0.4$, $R_d = N_t = N_b = M = 0.2, N = 0.5$ and $\lambda^* = M = \gamma = Q_H^* = K_H^* = 0$, at varying values of P_r.

$\mathbf{P_r}$	Rhman et al. [18]	Abbas et al. [20]	Qasim et al. [21]	Present study
0.07	0.87029	0.8701854	0.87018	0.870291
1.00	0.74417	0.7440651	0.74406	0.744173
6.70	0.29662	0.2966143	0.29661	0.296623
10.0	0.24216	0.2421726	0.24217	0.242161

3. RESULTS AND DISCUSSION

The study provides valuable insights into the role of nanofluids in cancer treatment, particularly in the context of thermal therapy. The discussion touches on several key parameters influencing the temperature distribution and nanoparticle (NP) concentration within the tumor, such as cylinder curvature (K), radiation parameters (R_d), thermophoresis, Brownian motion, and the use of magnetic fields**. Figures 2, 3**, and **4** are used to visually depict these effects, providing essential data on how these factors interact to influence therapeutic outcomes. Below is a detailed critical assessment of the discussion, focusing on the model assumptions, the clinical relevance of the findings, and their limitations.

One of the key assumptions in this study is the use of a steady-state model to analyze the governing equations. This approach is illustrated in the results presented in **Figure 2**, where the effects of parameters like cylinder curvature (K), radiation (R_d)), and constant velocity (γ) are explored under the assumption of steady-state conditions. Tumors are dynamic, and factors such as blood flow, tissue perfusion, and the diffusion of nanoparticles fluctuate over time, especially under the influence of therapeutic interventions like thermal therapy.

In **Figure 2**, the influence of cylinder curvature (K)on both the interstitial fluid temperature (θ) and NP concentration (φ) is highlighted. The results show that as K increases, both temperature and NP concentration rise, suggesting an enhancement in the delivery of NPs to the tumor. Another key limitation in the model is the assumption of uniform NP distribution within the tumor. **Figure 2(B**) shows that as cylinder curvature (K) increases, the NP concentration within the tumor rises. However, in reality, NP distribution within tumors is often highly heterogeneous, with some regions having poor vascularization that hinders NP uptake, while others may have regions of dense capillaries that allow better penetration. This variation in vascular permeability and the tortuosity of the tumor vasculature could significantly impact NP distribution.

A key observation in the study is that increasing the radiation parameter (R_d) leads to an increase in the temperature of the nanofluid but a decrease in NP concentration within the tumor **(Figure 2)**. This result aligns with the theoretical expectation that thermal radiation increases heat in the tumor, potentially improving the therapeutic effect. Also the increasing in radiation parameter leads to a thicker thermal boundary layer, which could reduce the diffusion of nanoparticles into the tumor.

In **Figure 2(C) and 2(D)**, the effect of (R_d) on temperature and NP concentration is visually represented, showing a significant increase in temperature but a reduction in NP concentration. Further exploration into the specific mechanisms causing this reduction would help to develop more effective strategies to optimize both heating and NP delivery. Moreover, the radiation parameters might vary depending on the tumor's location, depth, and optical properties, which should be considered for more accurate and personalized treatment models.

Figures 3(A) and 3(B) illustrate the contrasting effects of thermophoresis (N_t) and Brownian motion (N_b) on NP delivery. Thermophoresis enhances NP accumulation in the tumor by driving particles against the temperature gradient, while Brownian motion introduces random particle movement, reducing NP accumulation. This theoretical opposition is clearly depicted in **Figure 3**, where an increase in the thermophoresis parameter (N_t) results in a higher NP concentration in the tumor **(Figure 3(A))**, **(Figure 3(B)** whereas an increase in the Brownian motion parameter (N_b) reduces the NP concentration.

The effect of magnetic fields (M) on NP behavior is explored in **Figures 3(C)** and 3(D), which show that increasing the magnetic field parameter results in higher NP concentration and temperature within the tumor, improving treatment efficiency. Magnetic nanoparticles (MNPs) have been widely studied for their potential to be directed to specific tumor locations under the influence of an external magnetic field, and these results align with the theoretical benefits of magnetic targeting.

However, the clinical feasibility of using magnetic fields to manipulate NP delivery remains a significant challenge. Magnetic fields lose strength with distance, which limits their ability to precisely target deep tumors. Additionally, the heterogeneous nature of the body, including surrounding tissues and organs, may interfere with magnetic field distribution

In **Figure 3(E) and 3(F)**, the study discusses the effects of the particular absorption rate coefficient (λ^*) on both nanofluid temperature and NP concentration. The findings suggest that increasing (λ^*) results in higher temperatures, which is beneficial for thermal therapy but reduces NP concentration, potentially limiting drug delivery. This creates a trade-off between effective thermal treatment and efficient drug delivery, which is a key concern in Nanomedicines. The absorption rate coefficient could vary depending on the tumor's size, location, and stage, and future studies should explore how to adjust (λ^*) for personalized treatment protocols. By carefully managing the absorption rate, it might be possible to enhance both thermal therapy and NP delivery in a way that maximizes treatment efficacy while minimizing side effects.

Finally, the study's discussion on mixed convection (λ) and its effect on temperature and NP concentration **(Figure 4)** suggests that increasing (λ) decreases both the nanofluid temperature and NP concentration in the tumor. Tumors with different levels of vascularization and blood flow will respond differently to changes in convection, and this variability should be accounted for in treatment planning.

Furthermore, **Figure 4(C)** discusses the influence of radiation on the Nusselt number N_u across the vessel wall. As R_d increases, the Nusselt number decreases, indicating reduced heat transfer through the vessel wall. This finding suggests that convection might play a critical role in optimizing heat delivery to the tumor.

The study's findings provide several key insights that could be directly applied to the clinical optimization of cancer treatment using nanofluids in thermal therapy. From adjusting nanoparticle properties, tuning radiation levels, optimizing infusion velocities, and harnessing external magnetic fields, these strategies can be implemented to enhance drug delivery, tumor targeting, and treatment efficiency. By integrating these results into personalized treatment plans, clinicians can maximize the effectiveness of nanofluid-based thermal therapies in targeting tumors, improving patient outcomes while minimizing side effects.

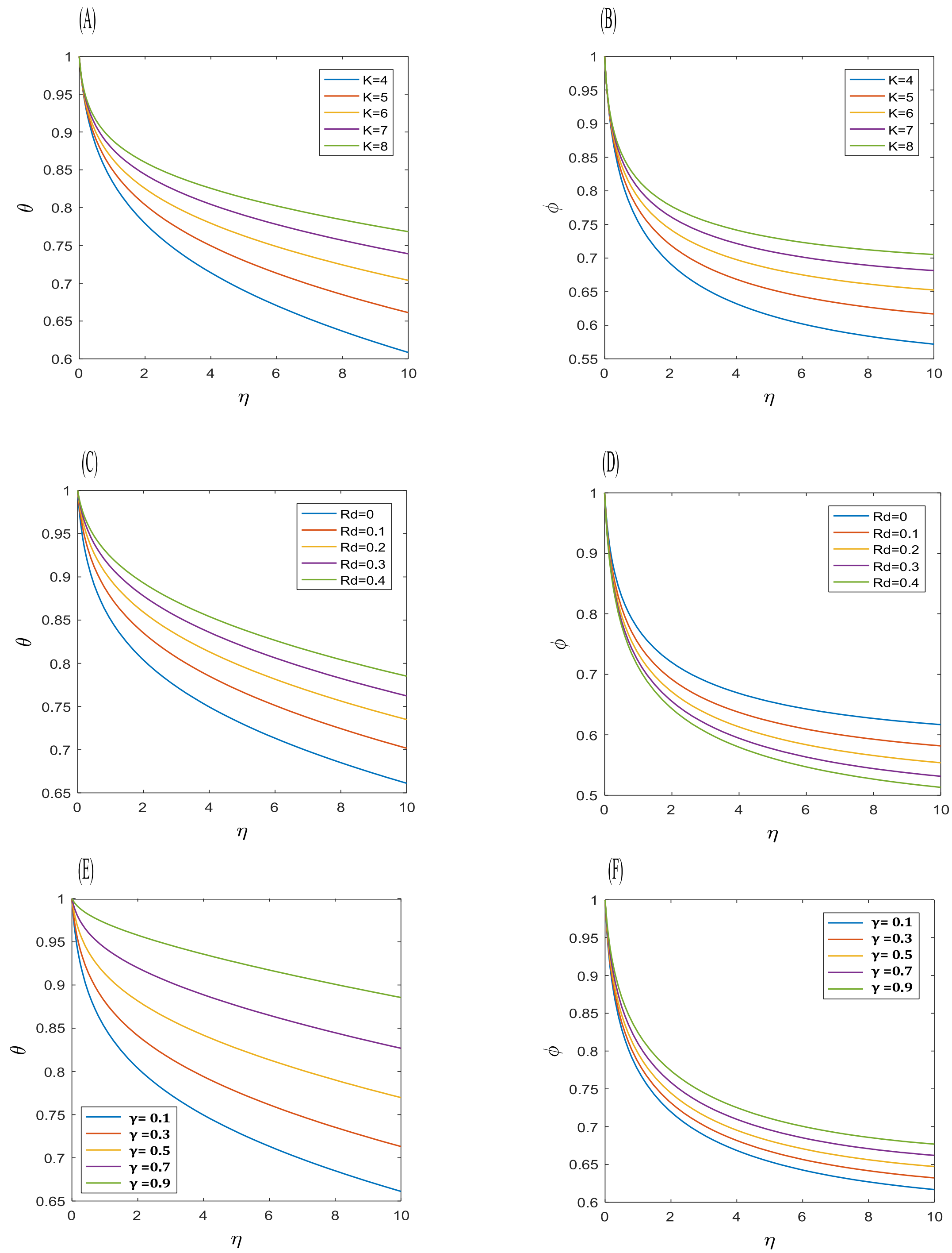

Figure 1: Nanofluid temperature and NP concentration. (A) The nanofluid temperature at different curvature values of $\mathbf{K}$, (B) Concentration of NPs for various curvature values of $\mathbf{K}$, (C) The nanofluid temperature for various values of $\mathbf{R_d}$, (D) Concentration of NPs for various values $\mathbf{R_d}$. (E) The nanofluid temperature for various values of $\boldsymbol{\gamma}$. (F) Nanofluid concentration for various values of $\boldsymbol{\gamma}$.

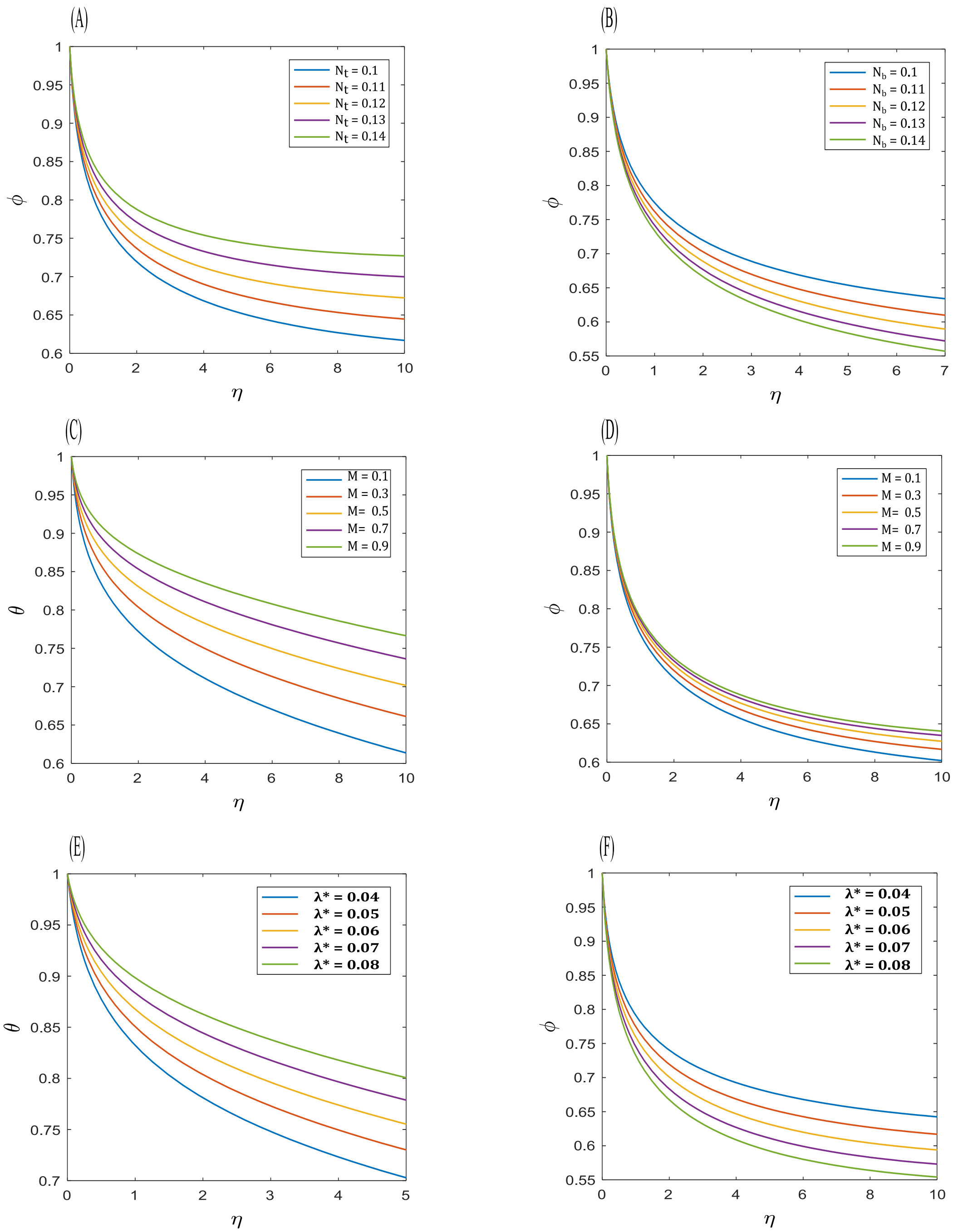

Figure 2: Nanofluid temperature and NP concentration. (A) Concentration of NPs for various values of $\mathbf{N_t}$, (B) Concentration of NPs for various values of $\mathbf{N_b}$, (C) The nanofluid temperature for various values of $\mathbf{M}$, (D) Concentration of NPs for various values of $\mathbf{M}$, (E) The nanofluid temperature for various values of $\boldsymbol{\lambda}^*$. (F) Concentration of NPs for various values of $\boldsymbol{\lambda}^*$.

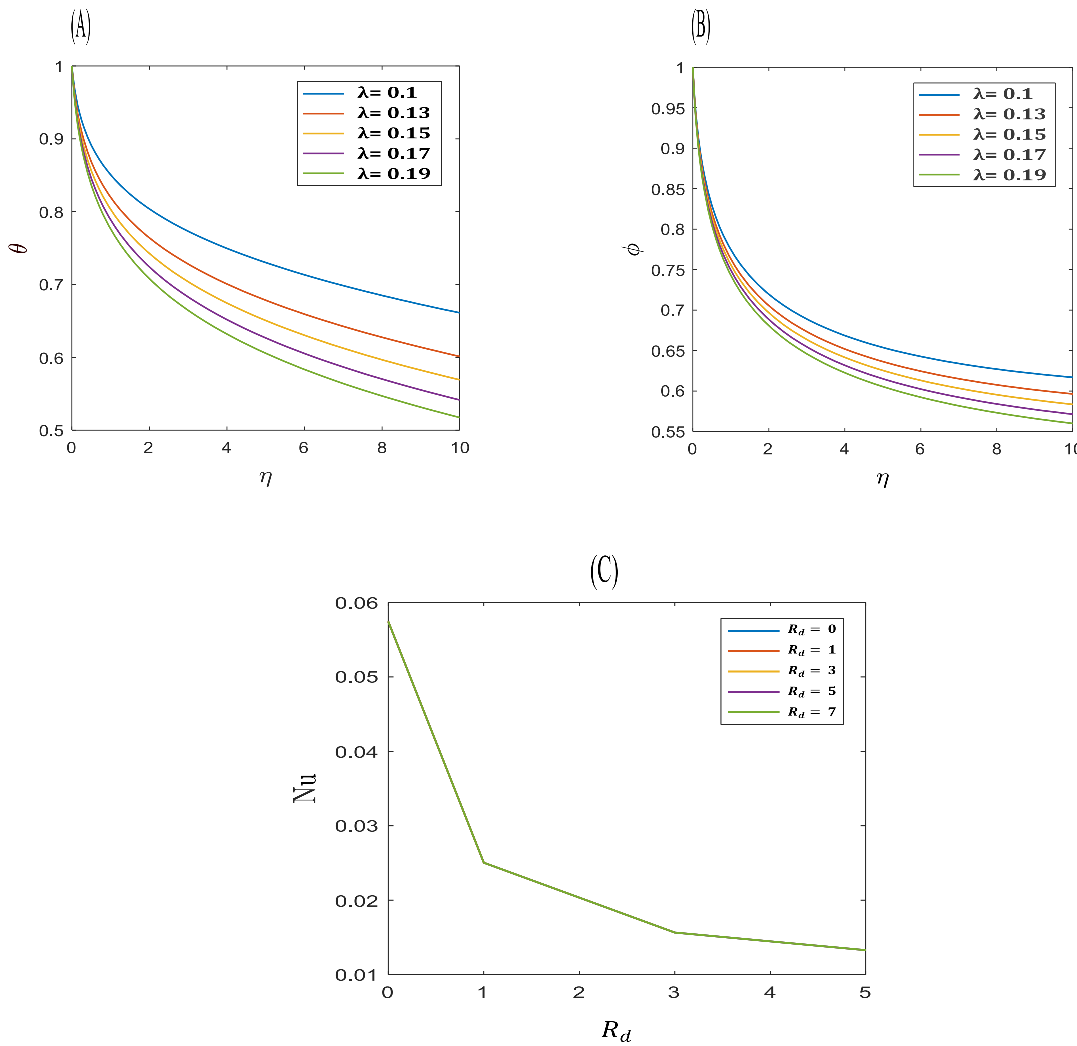

Figure 3: Nanofluid temperature, NP concentration and Nusselt number. **(A)** The nanofluid temperature for various values of λ, **(B)** Concentration of NP*s* for various values of λ, **(C)** The Nusselt number plotted against R_d.

4. CONCLUSION

The study explores how various physical parameters affect nanofluid behavior in tumor tissues, impacting the effectiveness of thermal therapy for cancer treatment. Key findings include the role of cylinder curvature, radiation, magnetic fields, fluid velocity, and thermophoresis in enhancing nanoparticle (NP) delivery and improving temperature profiles within tumors. These factors can boost treatment efficiency, while Brownian motion and mixed convection may hinder NP accumulation and heat retention, reducing therapy effectiveness.

The governing equations were solved numerically, allowing for detailed exploration of how factors such as cylinder curvature (K), radiation parameter R_d, dimensionless constant velocity (γ), thermophoresis parameter (N_t), Brownian motion parameter (N_b), magnetic field parameter (M), specific absorption rate coefficient λ^*, and mixed convection parameter (λ) influence interstitial fluid temperature and NP concentration.

Key findings indicate that:

- Increasing the curvature of the cylinder enhances NP accumulation within the tumor, and increase interstitial fluid temperature. Conversely, higher radiation parameters can lead to decreased NP concentration, which may reduce treatment efficacy.
- The influence of thermophoresis and Brownian motion further underscores the importance of understanding particle behavior within the tumor microenvironment. The results demonstrate that higher thermophoresis parameters can increase NP concentration, while increased Brownian motion leads to a reduction in NP concentration. The magnetic field parameter was found to enhance both temperature and NP concentration, improving treatment efficiency.

Overall, this study emphasizes the critical role of fluid dynamics and thermal properties in optimizing thermal therapy for cancer. The insights gained from this analysis can help in future research and clinical applications, guiding the development of more effective treatment strategies that leverage the unique properties of nanofluids. Future work should focus on further refining these models and exploring additional factors that may influence treatment efficacy.

Conflict of interest statement

The authors declare that they have no known competing financial interests or personal relationships that could have appeared to influence the work reported in this manuscript.

REFERENCES

[1] S.U. Choi and J.A. Eastman, Enhancing thermal conductivity of fluids with nanoparticles. Argonne, IL: Argonne NationalLab,1995.

[2] J. Buongiorno, Convective transport in nanofluids. J HeatTrans 2005;28(3):240–250.

[3] J.L. Sutterby, Laminar converging flow of dilute polymer solutions in conical sections II. Trans Soc Rheol 1965; 9(2): 227–241.

[4] A. Guha and K. Pradhan, Natural convection of non Newtonian power-law fluids on a horizontal plate. Int J Heat Mass Transf 2014; 70: 930–938.

[5] S. Bijjam, A. Dhiman and V. Gautam, Laminar momentum and heat transfer phenomena of power-law dilatant fluids around an asymmetrically confined cylinder. Int J Therm Sci 2015; 88: 110–127.

[6] S.I. Abdelsalam, R. Raza, and R. Naz, Microorganisms swimming through radiative Sutterby nanofluid over stretchable cylinder: hydrodynamic effect. Numerical Methods Partial Differ Equ 2023; 39(2): 975–994.

[7] U.r. Rahman, M. Rahman, F. Haq, M. Ijaz Khan F.A. Awwad, EAA. Ismail, Numerical assessment of irreversibility in radiated Sutterby nanofluid flow with activation energy and Darcy Forchheimer. Sci Rep. 2023 Nov 3;13(1):18982. doi: 10.1038/s41598-023-46439-8.

[8] A. Aldabesh, A. Haredy, K. Al-Khaled, S.U. Khan, I. Tlili, Darcy resistance flow of Sutterby nanofluid with microorganisms with applications of nano-biofuel cells. Sci Rep. 2022 May 7;12(1):7514. doi: 10.1038/s41598-022-11528-7.

[9] H. Fazal, S. Muzher, M. Khan Ijaz, Investigation of mixed convection magnetized Casson nanomaterial flow with activation energy and gyrotactic microorganisms, pub.1143065412 https://doi.org/10.1088/2399-6528/ac3889

[10] H. Zakir, H. Tasawar, A. Ahmed, U. Ikram U, On MHD convective flow of Williamson fluid with homogeneous-heterogeneous reactions: A comparative study of sheet and cylinder, 120, 2021, 105060.

[11] S. Bilal, M. Sohail, R. Naz, and M.Y. Malik, Dynamical and optimal procedure to analyze the exhibition of physical attributes imparted by Sutterby magneto-nanofluid in Darcy medium yielded by axially stretched cylinder. 2020 **98**(1): 1-10. https://doi.org/10.1139/cjp-2018-0581

[12] T. Hayat, Z. Hina, M. Mustafa, A. Alsaedi, Peristaltic flow of Sutterby fluid in a vertical channel with radiative heat transfer and compliant walls: A numerical study, 6, 2016, ISSN 2211-3797, https://doi.org/10.1016/j.rinp.2016.10.015.

[13] U.I. Ehsan, U.I. Sami, A. Tasawar, K. Smida, U.l. Hassan, B. Ahmad, M. Khan, K. Guedri, P. Kumam, Numerical aspects of thermos migrated radiative nanofluid flow towards a moving wedge with combined magnetic force and porous medium. (2022). http://dx.doi.org/10.1038/s41598-022-14259-x

[14] A.M. Ismaeel, M.A. Mansour, F.S. Ibrahim, F.M. Hady, Numerical simulation for nanofluid extravasation from a vertical segment of a cylindrical vessel into the surrounding tissue at the microscale, V. 417, 0096-3003, (2022).

[15] A.M. Ismaeel, R.S. Kamel, M.R. Hedar, Numerical simulation for a Casson nanofluid over an inclined vessel surrounded by hot tissue at the microscale. *SN Appl. Sci.* **5**, 223 (2023). https://doi.org/10.1007/s42452-023-05436-2.

[16] R.S. Kamel, A.M. Ismaeel, F.M. Hady, Numerical study for a Newtonian nanofluid over a vertical cylindrical vessel surrounded by a hot tissue. *SN Appl. Sci.* **5**, 315 (2023). https://doi.org/10.1007/s42452-023-05527-0.

[17] A. M. Ismaeel, R. S. Kamel, M. R. Hedar, & F. M. Hady, Numerical simulation of heat transfer and nanoparticle transport in a nanofluid within a tumour surrounding a blood vessel. Numerical Heat Transfer, Part A: Applications, 1–12. (2024)https://doi.org/10.1080/10407782.2024.2355515.

[18] M. Rahman , F. Haq, D. Abduvalieva, Mixed convection flow of radiated Sutterby nanofluid by stretchable cylinder with irreversibility and heat generation. 10.1177/23977914231223820 (2024). http://dx.doi.org/10.1177/23977914231223820

[19] W. Cai, N. Su, X. He, MHD convective heat transfer with temperature-dependent viscosity and thermal conductivity: a numerical investigation, Journal of Applied Mathematics and Computing, 52 , 305–321, (2016). http://dx.doi.org/10.1007/s12190-015-0942-2

[20] N. Abbas, W. Shatanawi and A. M. Taqi, Thermodynamic study of radiative chemically reactive flow of induced MHD Sutterby nanofluid over a nonlinear stretchingcylinder.AlexEngJ 2023;70:179–189.

[21] M. Qasim, Z.H. Khan, W.A. Khan, MHD boundary layer slip flow and heat transfer of ferro fluid along a stretching cylinder with prescribed heat flux .PLoS One 2014;9(6):e100462.

NOMENCLATURE

T_∞ Ambient Fluid Temperature (K)

D_B Brownian Motion Coefficient (m^2/s)

N_b Brownian Motion Parameter

K_H^* Coefficient of the Mean Absorption (m^{-1})

C_∞ Concentration in Ambient Flow

K Curvature of Cylinder

U, w Dimensionless Velocity Components

SAR External Specific Heat Resource

Q Heat Generation/Absorption Parameter

M Magnetic Field Parameter

B_0 Magnetic Field Strength $(kg \cdot s^{-2} \cdot A^{-1})$

C Nanoparticle Concentration

C_b Nanoparticle Concentration in Blood

N_u Nusselt Number

P_r Prandtl Number

m Power law index

Re_z Reynolds Number (Local)

S_c Schmidt Number

C_f Skin Friction Coefficient

C_p Specific Heat at Constant Pressure (Cp)

q_w Surface Heat Flux

T Temperature (K)

D_T Thermophoresis Coefficient (m^2/s)

N_t Thermophoresis Parameter

u, w Velocity Components in r, z Directions

Greek symbols

$\overline{K}$ Certain constant related to mass transfer

B Characteristic Time (s)

ρ Density (kg/m^3)

γ Dimensionless Constant Velocity

φ Dimensionless Nanoparticle Concentration

θ Dimensionless Temperature

μ Dynamic Viscosity

E_c Eckert Number

σ Electric Conductivity ($kg^{-1} \cdot m^{-3} \cdot s^3 \cdot A^2$)

Q_H^* Heat Flux

ν Kinematic Viscosity (m^2/s)

λ Mixed Convection Variable

R Radius of Cylinder

τ Ratio of the Heat Capacities of the Nanoparticles and the Base Fluid

λ^* Specific Heat Parameter

β Sutterby Fluid Parameter

N Thermal Buoyancy Ratio Variable

k Thermal Conductivity ($W \cdot m^{-1} \cdot K^{-1}$)

G_{r_z} Thermal Grashof Number

R_d Thermal Radiation Parameter

U_0 Radial Velocity at the Boundary

Subscripts

0 Reference

f Pure fluid

W Wall